Independent and continuous third-order dispersion compensation using a pair of prisms

Qingwei Yang, Xinglong Xie, Jun Kang, Haidong Zhu, Ailin Guo, and Qi Gao

National Laboratory on High Power Laser and Physics, Shanghai Institute of Optics and Fine Mechanics, Chinese Academy of Sciences, No. 390, Qinghe Road, Jiading District, Shanghai 201800, China

Abstract

The dispersion of a pair of prisms is analyzed by means of a ray-tracing method operating at other than tip-to-tip propagation of the prisms, taking into consideration the limited spectral bandwidth. The variations of the group delay dispersion and the third-order dispersion for a pair of prisms are calculated with respect to the incident position and the separation between the prisms. The pair of prisms can provide a wide range of independent and continuous third-order dispersion compensation. The effect of residual third-order dispersion on the pulse contrast ratio and pulse duration is also calculated. The residual third-order dispersion not only worsens the pulse contrast ratio, but also increases the pulse duration to the hundreds of femtosecond range for a tens of femtosecond pulse, even when the residual third-order dispersion is small. These phenomena are helpful in compensating for the residual high-order dispersion and in understanding its effect on pulse contrast ratios and pulse durations in ultrashort laser systems.

1. Introduction

The chirped pulse amplification (CPA) technique[1, 2] is commonly used to build high-power laser systems for various experiments and applications, such as laser-driven plasma accelerators and fast ignition in inertial confinement fusion. Peak laser powers of up to 1 PW (1 PW = 10^{15} W) are now achievable, and are expected to be boosted to the EW level (1 EW = 10^{18} W) in the near future[3].

In CPA ultrashort laser systems, the dispersion elements include stretcher, compressor and amplifier material[4–10]. The compressor can completely compensate for group delay dispersion (GDD) and partly compensate for third-order dispersion (TOD), which are generated by the stretcher and amplifier material[6, 7]. However, compensating for the residual high-order dispersion is extremely important in the entire system to obtain the shortest pulse duration and highest pulse contrast, particularly for ultrashort pulses (<50 fs)[3, 5]. Thus, setting up an independent dispersion compensation element is necessary to compensate for the residual high-order dispersion of the system.

The prism pair is an important element in dispersion compensation. In 1984, Fork *et al.* indicated that a pair of prisms

could provide negative GDD and TOD, which are suitable for the dispersion compensation element[11–14]. However, the equations used by Fork to evaluate the GDD and TOD of a pair of prisms are only for tip-to-tip propagation in the prisms and do not consider the effect of the spectral bandwidth. Another approach to evaluate the dispersion of a pair of prisms was presented by Arissian *et al.*[15, 16]; the technique is based on accurate calculation of the optical path of the pair of prisms. However, the equations employed by Arissian *et al.* to evaluate GDD and TOD of the pair of prisms do not consider limited spectral bandwidth and continuous TOD compensation, which are very important for dispersion compensation. For a particular ultrashort laser system, dispersion compensation can be considered to be quantitatively meaningful only under the premise of a certain spectral bandwidth; otherwise, this method is qualitative. For example, for a 30 fs ultrashort laser system, the spectral bandwidth of dispersion compensation should remain greater than 140 nm in order to obtain a short compressed pulse and a high pulse contrast ratio. But, in practical applications, the possible spectral bandwidth is only 30 nm when the spectral bandwidth is not considered in the dispersion compensation. In that time, a short compressed pulse (e.g., 30 fs) cannot be obtained. Therefore, it is very important to consider the

---

Correspondence to: Q. Yang, No. 390, Qinghe Road, Jiading District, Shanghai 201800, China. Email: yqwphy@siom.ac.cn
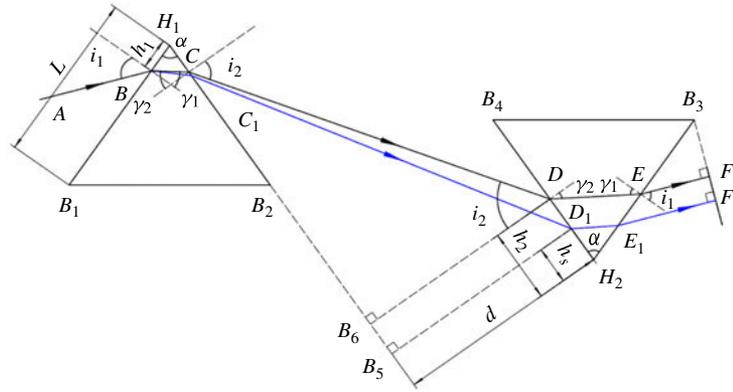
1

Figure 1. Ray-tracing sketch for a pair of identical isosceles prisms in a parallel face configuration.

spectral bandwidth in dispersion compensation, particularly in practical applications.

In this study, we focus on independent and continuous TOD compensation using a pair of prisms. The dispersion of the pair of prisms is analyzed in detail using a ray-tracing method operating at other than tip-to-tip propagation of the prisms. The variations of GDD and TOD for the pair of prisms are calculated with respect to the incident position and the separation between the prisms. A pair of prisms can provide a wide range of independent and continuous TOD compensation. The effect of residual TOD (RTOD) on the pulse contrast ratio and pulse duration is calculated. The RTOD not only worsens the pulse contrast ratio, but also greatly increases the pulse duration to the hundreds of femtosecond range for a tens of femtosecond pulse, even when small RTOD is employed. These phenomena are helpful in compensating for residual high-order dispersion and in understanding its effect on the pulse contrast ratio in ultrashort laser systems.

2. Model

Figure 1 shows the ray-tracing sketch for a pair of identical isosceles prisms in a parallel face configuration. The blue curve represents the shortest wavelength trajectory and the black curve represents any single wavelength trajectory after dispersion through the prism pairs.

Based on Figure 1, the optical path of any one wavelength is given by

$$
\begin{aligned}
p &= 2[n(BC + DE) + CD + EF] \\
&= 2\left\{ n\left[\frac{h_1 \sin \alpha}{\cos \gamma_2(\lambda)} + \frac{h_2 \sin \alpha}{\cos \gamma_1(\lambda)} \right] + \frac{d}{\cos i_2(\lambda)} \right. \\
&\quad \left. + \left[L - \frac{h_2 \cos \gamma_2(\lambda)}{\cos \gamma_1(\lambda)} \right] \sin i_1 \right\}
\end{aligned}
\tag{1}
$$

$$
h_2 = h_s + d \tan i_2(\lambda_s) - d \tan i_2(\lambda) + \frac{h_1 \sin \alpha}{\cos \gamma_2(\lambda_s)} - \frac{h_1 \sin \alpha}{\cos \gamma_2(\lambda)}
\tag{2}
$$

where λ is the wavelength under consideration, λ_s is the shortest wavelength, $n(\lambda)$ is the refractive index of the prism, h_1 is the distance of the beam input trajectory to the apex of the prism, h_2 is the distance of the trajectory at a particular wavelength to the apex of the second prism, h_s is the distance of the trajectory of the shortest wavelength to the apex of the second prism, L is the waist length of the isosceles prisms, α is the apex angle of the prism, i_1 is the incidence angle, $i_2(\lambda)$ is the exit angle of the prism, $\gamma_1(\lambda)$ is the refraction angle in the incidence plane, and $\gamma_2(\lambda)$ is the incidence angle in the exit plane of the first prism at a particular wavelength.

To ensure high transmission efficiency of the prism pairs, Brewster angle incidence is adopted. The values of these angles can be calculated using $i_1 = \arctan[n(\lambda_0)]$, $\gamma_1(\lambda) = \arcsin[\frac{\sin i_1}{n(\lambda)}]$, $\gamma_2(\lambda) = \alpha - \gamma_1(\lambda)$, $i_2(\lambda) = \arcsin[n(\lambda) \sin \gamma_2(\lambda)]$, where λ_0 is the central wavelength.
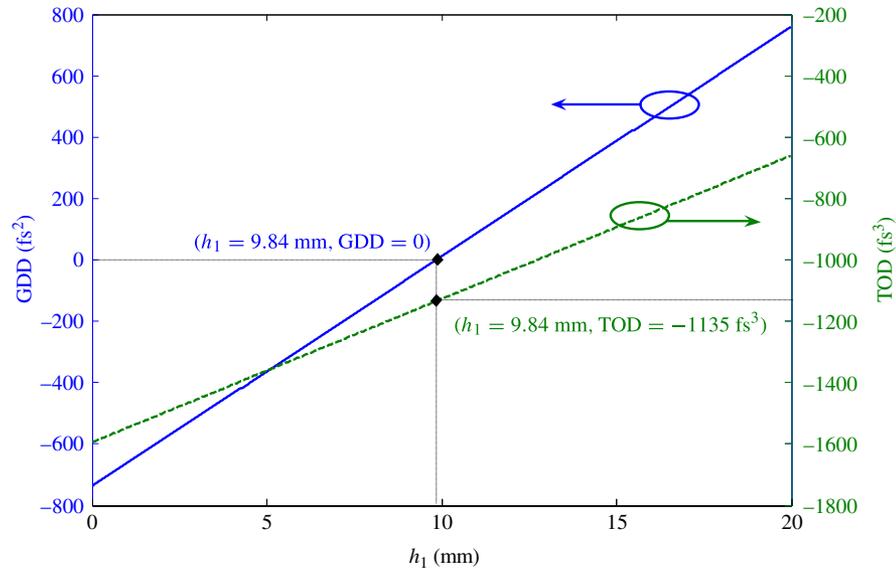
The total phase for the pair of prisms yields

$$
\phi(\omega) = \frac{\omega p}{c}
\tag{3}
$$

where ω is the angular frequency and c is the speed of light in vacuum.

According to Equation (3), the dispersions can be divided into various orders, such as the second-, third- and fourth-order dispersions (i.e., GDD, TOD and FOD, respectively).

$$
\text{GDD}|_{\omega_0} = \frac{\lambda^3}{2\pi c^2} \frac{d^2 P}{d\lambda^2} \bigg|_{\lambda_0}
\tag{4}
$$

$$
\text{TOD}|_{\omega_0} = -\frac{\lambda^4}{4\pi^2 c^3} \left(3\frac{d^2 P}{d\lambda^2} + \lambda \frac{d^3 P}{d\lambda^3} \right) \bigg|_{\lambda_0}
\tag{5}
$$

Figure 2. At the central wavelength, GDD and TOD change with h_1. Material: CaF_2; simulation parameters: $i_1 = 69.9°$, $\lambda_0 = 808$ nm, $\Delta\lambda = 140$ nm, $\lambda_s = 738$ nm, $d = 800$ mm, and $h_s = 1$ mm.

$$\text{FOD}|_{\omega_0} = \frac{\lambda^5}{8\pi^3 c^4} \left(12\frac{d^2 P}{d\lambda^2} + 8\lambda\frac{d^3 P}{d\lambda^3} + \lambda^2\frac{d^4 P}{d\lambda^4} \right)\Bigg|_{\lambda_0} \quad (6)$$

where ω_0 is the central angular frequency.

3. Numerical results

According to the model constructed in Section 2, we can calculate the GDD and TOD of the prisms. The influences of the distances h_1, h_s, and d on GDD and TOD are determined. We then discuss independent and continuous TOD compensation by changing the distances h_1 and d (or h_2 and d) simultaneously. The effect of RTOD on the pulse contrast ratio and pulse duration is also discussed.

During the simulation, we adopted a typical Sellmeier series equation to describe glass material dispersion[2]. The Sellmeier series equation is written as

$$n^2 = 1 + \frac{B_1\lambda^2}{\lambda^2 - C_1} + \frac{B_2\lambda^2}{\lambda^2 - C_2} + \frac{B_3\lambda^2}{\lambda^2 - C_3} \quad (7)$$

where the wavelength λ is expressed in µm. The Sellmeier coefficient values for $B_1, B_2, B_3, C_1, C_2, C_3$ are shown in Table 1.

3.1. Influence of distances h_1 and h_s on dispersion

At the central wavelength, GDD and TOD change with distance h_1 or h_s (Figures 2 and 3, respectively). GDD changes from negative to positive and TOD reduces rapidly when h_1 or h_s increases. For instance, when $h_1 < 9.84$ mm, the value of GDD is reduced rapidly (Figure 2). However,

when $h_1 > 9.84$ mm, the value of GDD increases rapidly. Thus, $h_1 = 9.84$ mm is the critical value; at $h_1 = 9.84$ mm, the value of GDD is zero and the value of TOD is -1135 fs^3. When $h_s < 11.7$ mm, the value of GDD reduces rapidly. However, when $h_s > 11.7$ mm, the value of GDD increases rapidly. Thus, $h_s = 11.7$ mm is the critical value; at $h_s = 11.7$ mm, the value of GDD is zero and the value of TOD is -1134 fs^3.

Figures 2 and 3 show that the simultaneous occurrence of GDD and TOD with the same or different signs is possible when h_1 or h_s changes. Therefore, the prisms can compensate for GDD and TOD with the same signs, as well as GDD and TOD with different signs, by changing h_1 or h_s.

In the simulation shown in Figure 2, the following parameters are employed: $i_1 = 69.9°$, $\lambda_0 = 808$ nm, $\Delta\lambda = 140$ nm, $\lambda_s = 738$ nm, $d = 800$ mm, and $h_s = 1$ mm; material: CaF_2.

In the simulation shown in Figure 3, the following parameters are employed: $i_1 = 69.9°$, $\lambda_0 = 808$ nm, $\Delta\lambda = 140$ nm, $\lambda_s = 738$ nm, $d = 800$ mm, and $h_1 = 1$ mm; material: CaF_2.
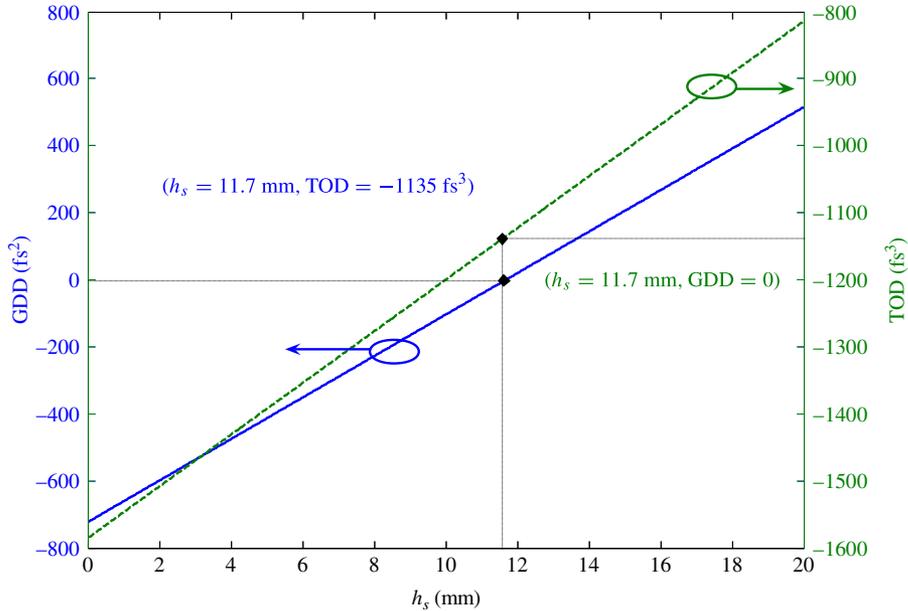
3.2. Influence of distance d on dispersion

At the central wavelength, GDD and TOD change with d (Figure 4). GDD and TOD change simultaneously from positive to negative with increasing d. For instance, when $d < 498.2$ mm, the value of GDD reduces rapidly. However, $d > 498.2$ mm, the value of GDD increases rapidly. Thus $d = 498.2$ mm is the critical value; at $d = 498.2$ mm, GDD is zero and TOD is -753 fs^3.
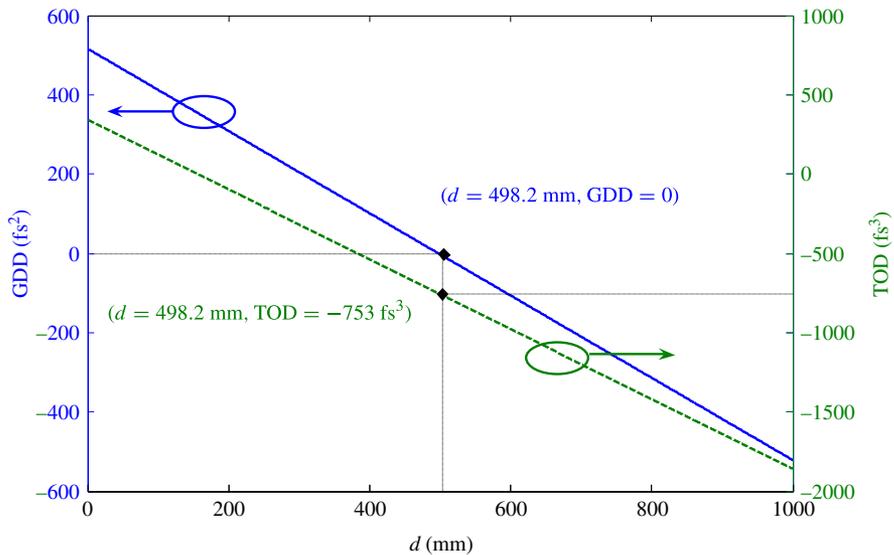
During the simulation, the following parameters are employed: $i_1 = 69.9°$, $\lambda_0 = 808$ nm, $\Delta\lambda = 140$ nm, $\lambda_s = 738$ nm, $h_1 = 6$ mm, and $h_s = 1$ mm; material: CaF_2.

Table 1. Sellmeier coefficients for Equation (7) obtained from the Thorlab catalog[17].

Material	B_1	B_2	B_3	C_1	C_2	C_3
CaF$_2$	5.67588800E−001	4.71091400E−001	3.84847230E+000	2.52643000E−003	1.00783330E−002	1.20055600E+003
SF10	1.61625977E+000	2.59229334E−001	1.07762317E+000	1.27534559E−002	5.81983954E−002	1.16607680E+002

Figure 3. At the central wavelength, GDD and TOD change with h_s. Material: CaF$_2$; simulation parameters: $i_1 = 69.9°$, $\lambda_0 = 808$ nm, $\Delta\lambda = 140$ nm, $\lambda_s = 738$ nm, $d = 800$ mm, and $h_1 = 1$ mm.
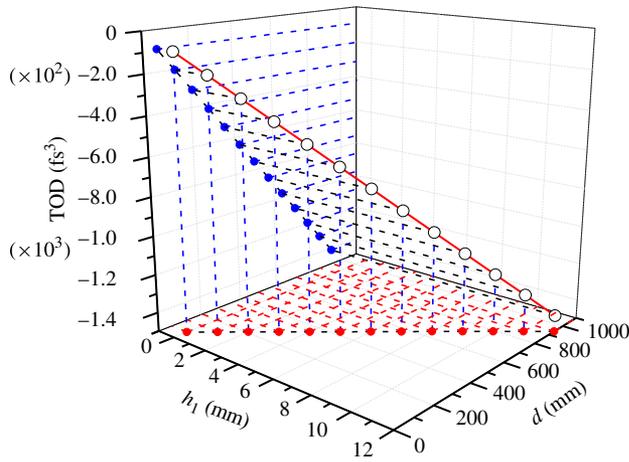

Figure 4. At the central wavelength, GDD and TOD change with d. Material: CaF$_2$; simulation parameters: $i_1 = 69.9°$, $\lambda_0 = 808$ nm, $\Delta\lambda = 140$ nm, $\lambda_s = 738$ nm, $h_1 = 6$ mm, and $h_s = 1$ mm.
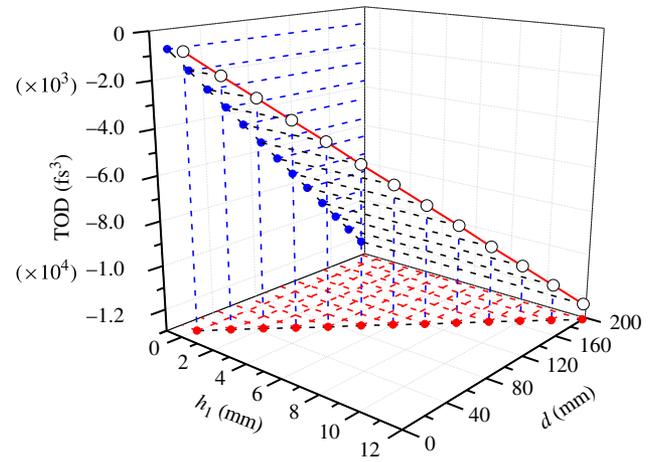
3.3. TOD independent and continuous compensation

Based on the analyses in Sections 3.1 and 3.2, we can conclude that the prisms can independently compensate for the TOD of the system by selecting the appropriate values of h_1 and d or h_s and d. At the central wavelength, TOD changes with h_1 and d when GDD = 0 (Figures 5 and 6). The figures indicate group-specific values (h_1, d)

Figure 5. At the central wavelength, TOD changes with h_1 and d when GDD = 0. Simulation parameters: $i_1 = 69.9°$, $\lambda_0 = 808$ nm, $\Delta\lambda = 140$ nm, $\lambda_s = 738$ nm, and $h_s = 1$ mm; material: CaF$_2$.

Figure 6. At the central wavelength, TOD changes with h_1 and d when GDD = 0. Simulation parameters: $i_1 = 60.6°$, $\lambda_0 = 808$ nm, $\Delta\lambda = 140$ nm, $\lambda_s = 738$ nm, and $h_s = 1$ mm; material: SF10.
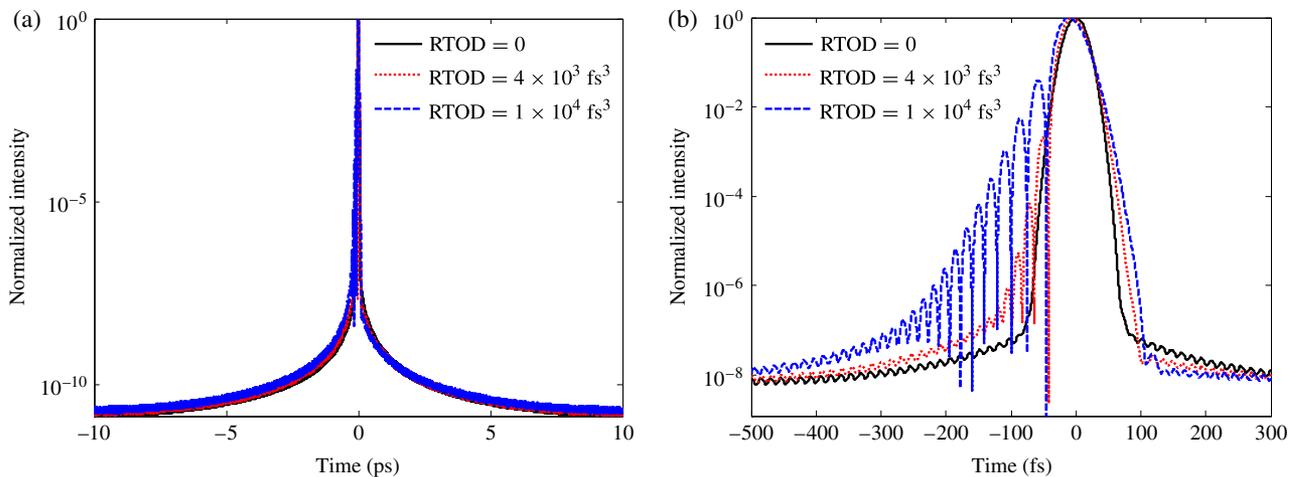
that correspond to a particular TOD compensation value. Thus, the RTOD of the laser system is compensated by adjusting distances h_1 and d simultaneously.

In the simulation shown in Figure 5, the following parameters are employed: $i_1 = 69.9°$, $\lambda_0 = 808$ nm, $\Delta\lambda = 140$ nm, $\lambda_s = 738$ nm, and $h_s = 1$ mm; material: CaF$_2$. In the simulation shown in Figure 6, the following parameters are employed: $i_1 = 60.6°$, $\lambda_0 = 808$ nm, $\Delta\lambda = 140$ nm, $\lambda_s = 738$ nm, and $h_s = 1$ mm; material: SF10. By comparison, we find that the CaF$_2$ prism pair can provide a smaller TOD, which is suitable for small RTOD compensation (Figure 5). By contrast, the SF10 prism pair can provide a larger TOD, which is suitable for large RTOD compensation (Figure 6) in the CPA laser system. The CaF$_2$ prisms are suitable for compensating RTOD under 10^3 fs^3, whereas the SF10 prisms are suitable for compensating RTOD under 10^4 fs^3.
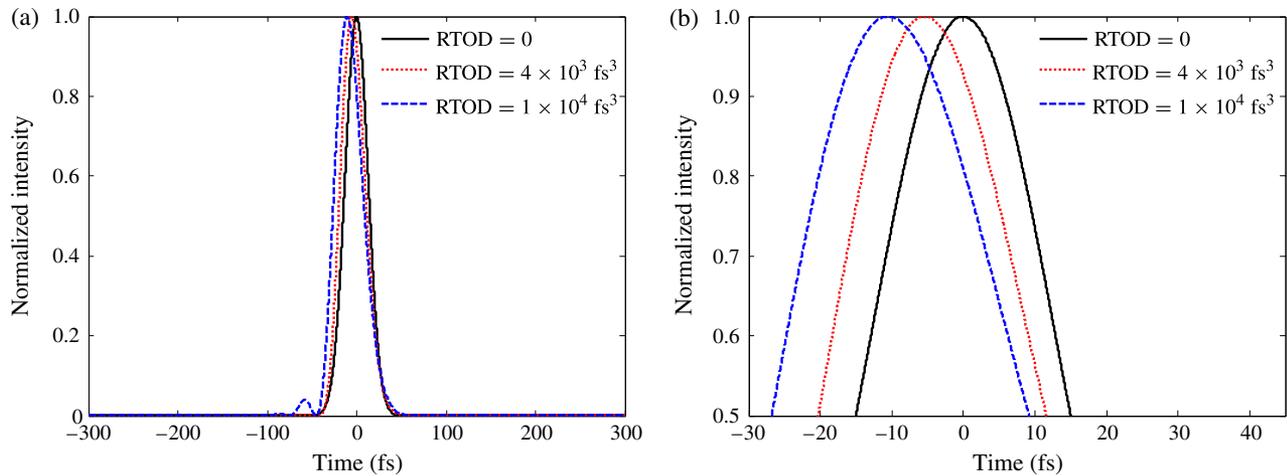
3.4. Effect of RTOD on pulse contrast ratio and pulse duration

To demonstrate the effect of RTOD on the pulse contrast in CPA lasers, we employed a 30 fs compressed pulse laser system as a example. The central wavelength is $\lambda_0 = 808$ nm and the spectral width is 140 nm. The spectral functions of the pulse exiting the compressor are assumed to have a Gaussian shape. The final output pulse contrast is calculated using a model in Ref. [2].

Figure 7 shows the effect of RTOD on the pulse contrast ratio. Even when RTOD is up to 10^4 fs^3, the output pulse contrast ratio in the 10 ps point is almost equal to the case when RTOD is zero (Figure 7(a)). However, the output pulse contrast ratios change in the range -300 to 300 fs (Figure 7(b)). For an ultrashort pulse (<50 fs), the RTOD not only affects the output contrast ratio, but also the pulse

Figure 7. Effect of RTOD on the pulse contrast ratio. (b) is a magnified section of (a).

Figure 8. Effect of RTOD on pulse duration. The figure on the right is a magnified section of the figure on the left.

duration from -300 to 300 fs. When RTOD is 1×10^4 fs^3, the output pulse duration is increased from 30 to 36 fs (Figure 8).

4. Conclusion

In summary, a ray-tracing model is presented to calculate the dispersion of a pair of prisms operating at other than tip-to-tip propagation of the prisms. The pair of prisms can provide a wide range of independent and continuous TOD compensation by employing appropriate values of h_1 and d or h_s and d simultaneously, which is helpful in compensating the residual high-order dispersion of the CPA laser system. RTOD not only worsens the pulse contrast ratio, but also increases the pulse duration to the hundreds of femtosecond range for a tens of femtosecond pulse, even at small RTOD. These phenomena are helpful in understanding the effect of residual high-order dispersion on the pulse contrast ratio in ultrashort pulse laser systems.

Acknowledgements

References

1. D. Strickland and G. Mourou, Opt. Commun. **56**, 219 (1985).
2. G. A. Mourou, T. Tajima, and S. V. Bulanov, Rev. Mod. Phys. **78**, 309 (2006).
3. http://www.extreme-light-infrastructure.eu.
4. G. Cheriaux, P. Rousseau, F. Salin, and J. P. Chambaret, Opt. Lett. **21**, 414 (1996).
5. S. Backus, C. G. Durfee III, M. M. Murnane, and H. C. Kapteyn, Rev. Sci. Instrum. **69**, 1207 (1998).
6. E. B. Treacy, IEEE J. Quantum Electron. **QE-5**, 454 (1969).
7. Q. Yang, A. Guo, X. Xie, F. Zhang, M. Sun, Q. Gao, M. Li, and Z. Lin, Rev. Laser Eng. **36 (APLS)**, 1053 (2008).
8. Q. Yang, M. Liu, Y. Wang, X. Xie, A. Guo, and Z. Lin, Optik **123**, 1704 (2012).
9. Q. Yang, A. Guo, X. Xie, F. Zhang, M. Sun, Q. Gao, M. Li, and Z. Lin, Optik **121**, 696 (2010).
10. Q. Yang, M. Liu, Y. Wang, X. Xie, M. Sun, T. Xu, Q. Gao, A. Guo, and Z. Lin, Chin. Opt. Lett. **10**, S21401 (2012).
11. R. L. Fork, O. E. Martinez, and J. P. Gordon, Opt. Lett. **9**, 150 (1984).
12. R. E. Sherriff, J. Opt. Soc. Am. B **15**, 1224 (1998).
13. R. Zhang, D. Pang, J. Sun, Q. Wang, S. Zhang, and G. Wen, Opt. Laser Technol. **31**, 373 (1999).
14. E. Cojocaru, Appl. Opt. **42**, 6910 (2003).
15. L. Arissian and J. C. Diels, Phy. Rev. A **75**, 013814.1 (2007).
16. C. Y. R. Corral, M. R. Aguilar, and J. G. Mejia, J. Mod. Opt. **56**, 1659 (2009).
17. http://www.thorlabschina.cn/newgrouppage9.cfm?objectgroup_id=3242.